FINAL REPORT

UPDATE OF THE PROBABILISTIC SEISMIC HAZARD ANALYSIS AND DEVELOPMENT OF SEISMIC DESIGN GROUND MOTIONS AT THE LOS ALAMOS NATIONAL LABORATORY

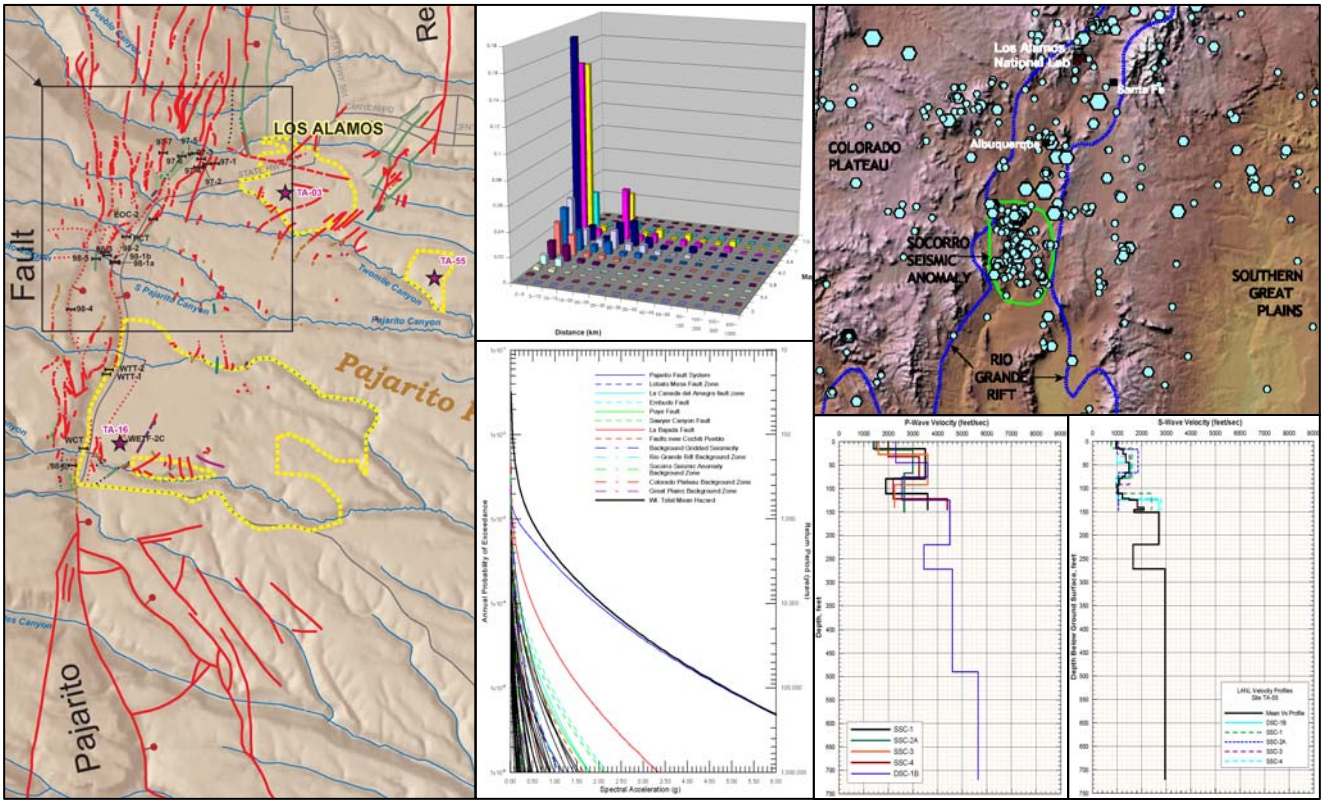

Prepared for
Los Alamos National Laboratory

25 May 2007

Prepared by
Ivan Wong, Walter Silva, Susan Olig, Mark Dober, Nick Gregor, Jamie Gardner, Claudia Lewis, Fabia Terra, Judith Zachariasen, Kenneth Stokoe, Patricia Thomas, and Shobhna Upadhyaya

As a subcontractor to Burns and Roe Enterprises, Inc.

URS Corporation
Seismic Hazards Group
1333 Broadway, Suite 800
Oakland, California 94612

Job No. 24342433

At the request of the Los Alamos National Laboratory (LANL), URS Corporation and Pacific Engineering & Analysis (PE&A), with support from the Earth and Environmental Sciences Division at LANL, have updated the 1995 probabilistic seismic hazard analysis (PSHA) of LANL (Wong *et al.*, 1995), and developed Design/Evaluation Basis Earthquake (DBE) ground motion parameters. Both Uniform Hazard Response Spectra (UHRS) and Design Response Spectra (DRS) have been calculated per ASCE/SEI 43-05 for the site of the Chemistry and Metallurgical Research Replacement (CMRR) building and for Technical Areas TA-3, TA-16, and TA-55. Site-wide and reference rock-outcrop (dacite) ground motions have also been developed and are recommended for use in the design of facilities in other Technical Areas. DRS were computed for Seismic Design Categories (SDC)-3 (2,500-year return period), -4 (2,500 years), and -5 (10,000 years).

The PSHA was conducted following the guidelines of the Senior Seismic Hazard Analysis Committee for a Level 2 PSHA. Principal inputs required for the development of the DBE ground motions include a seismic source model, ground motion attenuation relationships, and velocity and nonlinear dynamic properties of the lower Quaternary (1.2 to 1.6 Ma) Bandelier Tuff beneath each site.

Since 1995, the only new geotechnical, geologic, and geophysical data available to characterize the dynamic properties of the subsurface geology beneath LANL, particularly the Bandelier Tuff, are the results of investigations performed at the CMRR site. Downhole-velocity, OYO-suspension velocity, and seismic crosshole surveys were performed in boreholes drilled in 2005 at that site. The boreholes include four shallow holes at the corners of the proposed CMRR building footprint (SSC-1 to SSC-4), one deep hole in the center of the footprint (DSC-1B), and a deep hole outside and to the east of the footprint (DSC-2A). Dynamic laboratory testing was also performed by the University of Texas at Austin (UTA) on 22 samples collected in the CMRR boreholes. The dynamic properties that were evaluated are the strain-dependent shear modulus (G) and material damping ratio (D) of the samples. Based principally on the new CMRR data and data collected in 1995, base-case profiles of low-strain shear-wave velocity (V_S) and compressional-wave velocity (V_P) were developed for the CMRR, TA-3, TA-16, and TA-55 sites. Of particular significance to the site response analysis was the existence of the geologic unit Qbt3L, a low-velocity zone within the Bandelier Tuff. Unit-specific shear-modulus reduction and damping curves were developed on the basis of the dynamic laboratory testing results, including the 1995 testing. One set of curves for each unit was corrected for sample disturbance by adjusting reference strains by the ratio of laboratory-to-field V_S measurements.

The 50-km-long Pajarito fault system (PFS) extends along the western margin of LANL and is the dominant contributor to the seismic hazard at the laboratory because of its close proximity and rate of activity. The current (or new) characterization of the PFS is significantly revised from the 1995 study in order to incorporate a considerable amount of new mapping, displacement measurements, and paleoseismic data for the PFS. The PFS is a broad zone of faults that form an articulated monoclinal flexure, which consists of several distinct fault segments that have linked together. The PFS exhibits complex rupture patterns and shows evidence for at least two, probably three surface-faulting earthquakes since 11 ka. This recent temporal clustering of events is in contrast to evidence for the occurrence of only six to nine events since 110 ka although this longer record is likely incomplete. For the new analysis, both segmented and unsegmented rupture models were considered for the PFS, favoring the latter

which is characterized by a 36-km-long, floating earthquake rupture source. Two types of multisegment ruptures for the PFS were also considered: simultaneous (a single large earthquake) and synchronous (two subevents). The preferred range of maximum earthquakes is from moment magnitude (**M**) 6.5 to 7.3. Recurrence rates are dependent on rupture model and both long-term slip rate and late Quaternary recurrence interval data were considered. For the preferred unsegmented rupture model, the weighted-mean slip rate was 0.21 mm/yr, and weighted mean recurrence intervals were 4,400 years (for the logic tree branch assuming temporal clustering) and 17,600 years (for the not-in-a-cluster branch). For the segmented rupture model, a moment-balancing approach was used similar to that used by the Working Group on California Earthquake Probabilities (2003) to partition the slip rate of a segment into earthquakes representing various rupture scenarios and to keep the fault in moment equilibrium. Thus, rates vary for each rupture scenario but overall were consistent with the long-term slip rates of the segmented rupture model.

In addition to the dominant PFS, 55 additional fault sources were included in the PSHA. Parameters that were characterized for each fault include: (1) rupture model including independent versus dependent, single plane versus zone, segmented versus unsegmented, and linked configurations; (2) probability of activity; (3) fault geometry including rupture length, rupture width, fault orientation, and sense of slip; (4) maximum magnitude (**M**); and (5) earthquake recurrence, including both recurrence models and rates (using recurrence intervals and/or fault slip rates). There are sparse data on rates of activity for many faults so the approach developed by McCalpin (1995) was applied to characterize fault slip rate distributions. McCalpin's analysis was updated, adding 15 slip rate observations from six additional faults.

In addition to active faults, three areal earthquake source zones were defined based on seismotectonic provinces in the LANL region: the Rio Grande rift, Southern Great Plains, and Colorado Plateau. Due to its high level of seismicity, the Socorro Seismic Anomaly was also modeled as an areal source zone and differentiated from the Rio Grande rift. Earthquake recurrence rates computed for each areal source zone are based on an updated (through 2005) historical seismicity catalog. In addition to the traditional approach of using areal source zones, Gaussian smoothing with a spatial window of 15 km was used to address the hazard from background seismicity and to incorporate a degree of stationarity. The two approaches, areal sources and Gaussian smoothing were weighted equally to compute the hazard from background seismicity in the PSHA.

A combination of both empirical and site-specific attenuation relationships were used in the PSHA. The empirical models were weighted as follows: Abrahamson and Silva (1997), modified for normal faulting, 0.45; Spudich *et al.* (1999), 0.35; Campbell and Bozorgnia (2003), 0.10; Sadigh *et al.* (1997), 0.05; and Boore *et al.* (1997), 0.05. The relationships were weighted based on their appropriateness for the extensional Rio Grande rift. Because the epistemic variability was deemed insufficient as provided by the five attenuation relationships, they were all scaled to obtain a total sigma (ln) of 0.4.

To compensate for the lack of region-specific attenuation relationships, the stochastic ground motion modeling approach was used, as it was in 1995, to develop site-specific relationships for LANL. The point-source version of the stochastic methodology was used to model earthquakes from **M** 4.5 to 8.5 in the distance range of 1 to 400 km. To accommodate finite-source effects at large magnitudes (**M** > 6.5), model simulations included an empirical magnitude-dependent

short-period saturation as well as a magnitude-dependent far-field fall off. Relationships were developed for the CMRR, TA-3, TA-16, and TA-55 sites. A relationship for dacite was also developed. Aleatory variabilities in stress drop, magnitude-dependent point-source depths, the crustal attenuation parameters Q_o and η, and kappa were included in the computations of the attenuation relationships through parametric variations. Site-specific profiles (low-strain V_S, and V_P down to dacite) as well as modulus-reduction and hysteretic-damping curves were also randomly varied.

Variability (aleatory) in the regression of the simulated data is added to the modeling variability to produce 16th, 50th (median), and 84th percentile attenuation relationships. Thirty simulations were made for each magnitude and distance, and the results fitted with a functional form that accommodates magnitude-dependent saturation as well as far-field fall-off. Twelve attenuation relationships developed for the CMRR site were derived from three stress drops, two velocity models, and two sets of dynamic material properties. For the TA-3, TA-16, and TA-55 sites there were nine attenuation relationships derived from three stress drops, one velocity profile, and three sets of dynamic curves. There were six attenuation relationships for dacite derived from one profile, two sets of dynamic curves, and three stress drops.

In the 1995 study, attention was focused on potential topographic effects on ground motions due to the location of LANL facilities on mesas. In this study, a suite of topographic amplification factors was developed for LANL on the basis of (1) recent LANL modeling results, (2) other modeling results and observations in the literature, and (3) recommendations of Eurocode 8. The amplification factors are based on slope angles following Eurocode 8 as well as the French Seismic Code. To accommodate a fully probabilistic hazard analysis, both median estimates and standard deviations were developed, based on ranges of factors in modeling results and observations.

Probabilistic seismic hazard was calculated for the ground surface at CMRR, TA-3, TA-16, TA-55 and the top of dacite at TA-55. The hazard from the site-specific stochastic and empirical western U.S. soil attenuation relationships was calculated separately for each type of relationship. The modeling shows that the probabilistic hazard for peak horizontal ground acceleration (PGA) at all the above sites is controlled primarily by the PFS at all return periods. The PFS similarly controls the hazard at LANL for longer-period ground motions, such as 1.0 sec spectral acceleration (SA). Background seismicity in the Rio Grande rift, which contributed to the hazard at LANL in the 1995 study, is not a significant contributor in this new analysis, probably due to the increased activity rate of the PFS in the Holocene (clustering).

In calculating the probabilistic ground motions at LANL, the surface motions must be hazard consistent; that is, the annual exceedance probability of the soil UHRS should be the same as the rock UHRS. In NUREG/CR-6728, several site response approaches are recommended for use to produce soil motions consistent with the rock outcrop hazard. These approaches also incorporate site-specific aleatory variabilities of soil properties into the soil motions. To compute the site-specific ground-shaking hazard at LANL, we used two different approaches: (1) empirical attenuation relationships for the western U.S. (WUS) generic deep firm soil and (2) site-specific attenuation relationships. In the case of the latter, the site response is contained in the stochastic attenuation relationships (Approach 4). For the empirical attenuation relationships, the

computed generic soil hazard curves from the PSHA were adjusted for the site-specific site conditions at each of the LANL sites using computed amplification factors (Approach 3).

The point-source version of the stochastic ground motion model was used to generate the amplification factors (the ratios of the response spectra at the top of the site profiles to the WUS soil). They are a function of the reference (WUS deep firm soil) peak acceleration, spectral frequency, and nonlinear soil response. Amplification factors were computed for CMRR (4 sets), TA-3 (3 sets), TA-16 (3 sets), and TA-55 (3 sets), based on the velocity profiles and properties, but only one set was computed for the top of dacite. The point-source stochastic model was also used to compute site-specific vertical-to-horizontal (V/H) ratios. To accommodate model epistemic variability following the approach used for the horizontal hazard analyses, empirical deep firm soil V/H ratios were also used with equal weights between the stochastic and empirical models.

The hazard curves derived from the empirical attenuation relationships and the amplification factors were used to calculate site-specific hazard curves using Approach 3. These hazard curves and the hazard curves based on site-specific stochastic attenuation relationships (Approach 4) were then weighted equally and the topographic amplification factors and V/H ratios were applied. In seismic hazard analyses, epistemic uncertainty (due to lack of knowledge) of parameters and models is typically represented by a set of weighted hazard curves. Using these sets of curves as discrete probability distributions, they can be sorted by the frequency of exceedance at each ground-motion level and summed into a cumulative probability mass function. The weighted-mean hazard curve is the weighted average of the exceedance frequency values.

Based on the final site-specific hazard curves, mean horizontal UHRS were computed for CMRR, TA-3, TA-16, and TA-55. The TA-55 UHRS is based on an envelope of the hazard curves of CMRR and the hazard curve developed on basis of the 1995 borehole velocity profiles (SHB-1). Dacite and site-wide mean horizontal UHRS were also computed. The site-wide UHRS is derived from an envelope of the hazard curves of CMRR, TA-3, TA-16, and TA-55. Table ES-1 lists the horizontal and vertical PGA values for the UHRS.

The new PSHA shows that the horizontal surface PGA values are about 0.5 g at a return period of 2,500 years. The vertical PGA values at the same return period are about 0.3 g. The 1995 horizontal PGA values for a return period of 2,500 years are about 0.33 g. The estimated hazard has increased significantly (including other spectral values) from the 1995 study due to the increased ground motions from the site-specific stochastic attenuation relationships and increase in the activity rate of the PFS. The site response effects as modeled in this study with the newer site geotechnical data appears to amplify ground motions more than in the 1995 analysis. Other factors could be the increased epistemic uncertainty incorporated into the empirical attenuation relationships and in the characterization of the PFS.

Horizontal and vertical DRS for CMRR, TA-3, TA-16, TA-55, dacite, and site-wide were calculated for SDC-3, -4, and -5. Table ES-2 lists the horizontal and vertical PGA values for the DRS. DRS at other dampings levels of 0.5%, 1%, 2%, 3%, 7%, and 10% were computed from the 5%-damped DRS using empirical damping ratios.

Strain-compatible properties including V_S, V_S sigma, S-wave damping, S-wave damping sigma, V_P, V_P sigma, P-wave damping, and strains as a function of depth were calculated for return periods of 2,500 and 10,000 years. The strain-compatible properties are consistent with the mean hazard.

Time histories were developed through spectral matching following the recommended guidelines contained in NUREG/CR-6728. The phase spectra were taken from accelerograms of the 23 November 1980 (1934 GMT) **M** 6.9 Irpinia, Italy, earthquake recorded at the Sturno strong motion site.

Table ES-1
LANL Mean PGA Values (g) From the UHRS

Return Period (years)	CMRR		TA-3		TA-16		TA-55		Site-Wide		Dacite	
	Horiz.	Vert.	Horiz.	Vert.	Horiz.	Vert.	Horiz.	Vert.	Horiz.	Vert.	Horiz.	Vert.
1,000	0.27	0.32	0.27	0.32	0.25	0.31	0.27	0.32	0.27	0.32	0.13	0.12
2,500	0.52	0.60	0.52	0.59	0.47	0.57	0.52	0.60	0.52	0.60	0.27	0.27
10,000	1.03	1.21	1.03	1.10	0.93	1.05	1.03	1.21	1.03	1.21	0.65	0.65
25,000	1.47	1.79	1.45	1.57	1.33	1.50	1.47	1.79	1.47	1.79	1.01	0.97
100,000	2.30	3.01	2.29	2.79	2.11	2.57	2.30	3.01	2.30	3.01	1.69	1.65

Table ES-2
LANL PGA Values (g) From the DRS

SDC	CMRR		TA-3		TA-16		TA-55		Site-Wide		Dacite	
	Horiz.	Vert.	Horiz.	Vert.	Horiz.	Vert.	Horiz.	Vert.	Horiz.	Vert.	Horiz.	Vert.
3	0.47	0.56	0.47	0.53	0.43	0.50	0.47	0.60	0.47	0.56	0.28	0.27
4	0.72	0.87	0.71	0.78	0.65	0.74	0.72	0.86	0.72	0.86	0.47	0.45
5	1.17	1.50	1.17	1.39	1.07	1.29	1.17	1.50	1.17	1.50	0.84	0.82

SDC = Seismic Design Category

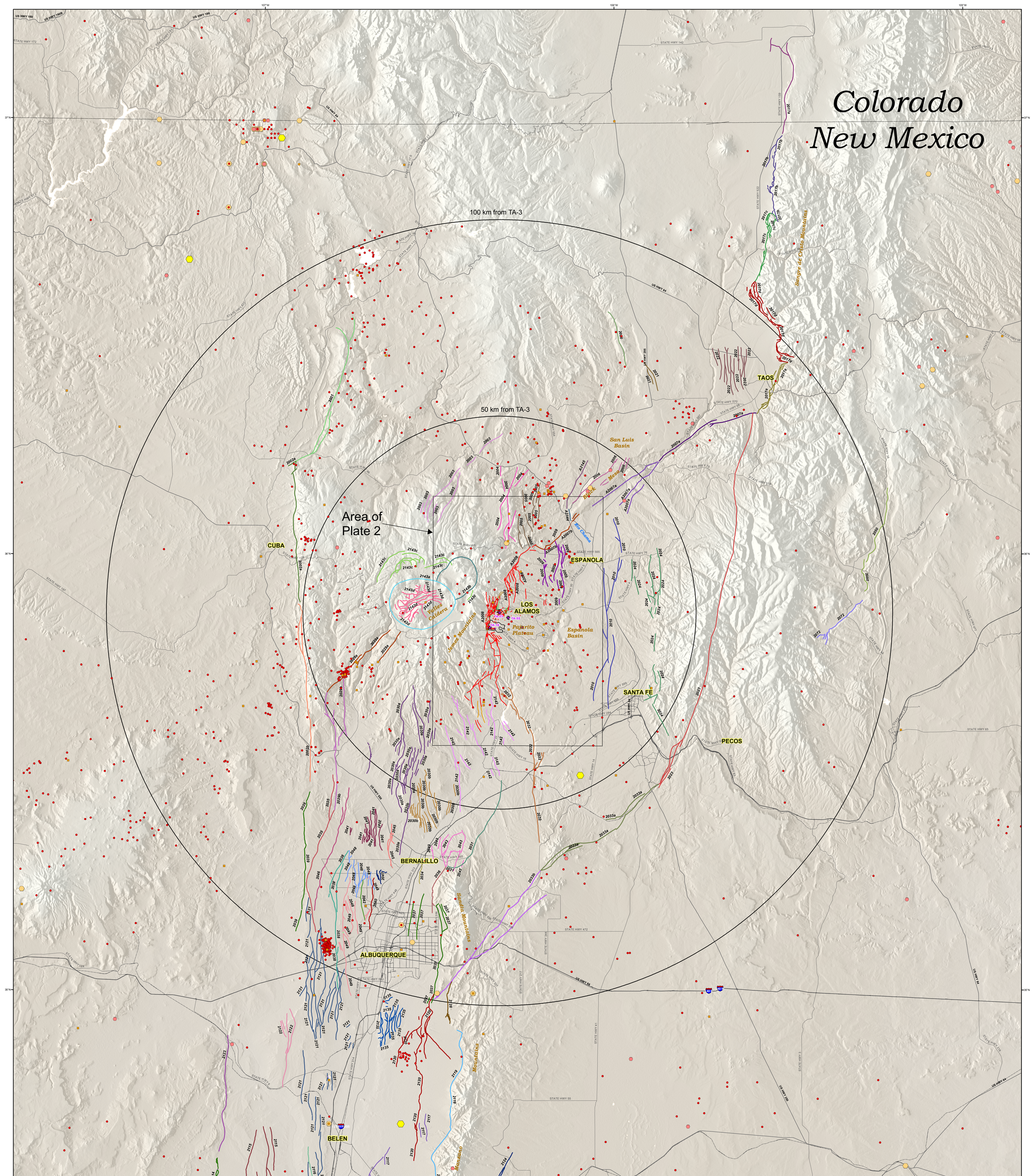

Pajarito Fault System (A2008)[1] (modified from Lewis et al., 2005)

- fault
- fault (assumed/uncertain)
- fault (concealed)
- fault (located approximately)
- fault zone
- fissure
- fissure (located approximately)
- monocline, bottom hinge
- monocline, bottom hinge (approximate)
- monocline, bottom hinge (concealed)
- monocline, top hinge
- monocline, top hinge (approximate)
- monocline, top hinge (concealed)
- syncline
- Fault from Machette et al. (1988), originally included as 2124, but included here as part of A2008

[1] Replaces faults: 2008 (Pajarito), 2026 (Rendija Canyon), 2027 (Guaje Mountain) and 2028 (Sawyer Canyon) of Machette et al. (1998)

TA-3 ★ Site Where Vibratory Ground Motions are Calculated

N

0 10 20 30 Kilometers

Faults from the USGS Quaternary Fault Database [2]

- 2001, Gallina fault
- 2002a, Nacimiento fault, northern section
- 2002b, Nacimiento fault, southern section
- 2003, Canones fault
- 2004, Lobato Mesa fault zone
- 2005, La Canada del Amagre fault zone
- 2006, Black Mesa fault
- 2007a, Embudo fault zone, northeastern section (Partially replaced with A2007a from Koning et al. 2004)
- 2009, Puye fault
- 2010, Pojoaque fault zone
- 2017a, Southern Sangre de Cristo fault zone, San Pedro Mesa section
- 2017b, Southern Sangre de Cristo fault, Urraca section
- 2017c, Southern Sangre de Cristo fault; Questa section
- 2017d, Southern Sangre de Cristo fault, Hondo section
- 2017e, Southern Sangre de Cristo fault, Canon section
- 2020, Las Tablas fault
- 2021, Joe Glenn Ranch faults
- 2021, Stong fault
- 2022, Los Cordovas fault
- 2023, Picuris-Pecos fault
- 2024, Nambe fault
- 2029a, Jemez-San Ysidro fault, Jemez section
- 2029b, Jemez-San Ysidro fault, San Ysidro section
- 2030a, San Felipe fault zone, Santa Ana section
- 2030b, San Felipe fault, Algodones section
- 2031, San Francisco fault
- 2032, La Bajada fault
- 2033a, Tijeras-Canoncito fault, Galisteo section
- 2033b, Tijeras-Canoncito fault, Canyon section
- 2034, Bernalillo fault
- 2035, Calacillas fault
- 2036, Rincon fault
- 2037, Sandia fault
- 2038, County Dump fault
- 2039, Sand Hill fault zone
- 2040, East Paradise fault zone
- 2041, Unnamed faults near Picuda Peak
- 2042, West Paradise fault zone
- 2043, Faults north of Placitas
- 2045, Unnamed faults near Loma Barbon
- 2046, Zia fault
- 2047, Unnamed faults near Loma Colorado de Abajo
- 2048, Unnamed faults near Star Heights
- 2049, Unnamed faults near Albuquerque Volcanoes
- 2050, El Oro fault
- 2050, Unnamed faults near Albuquerque Volcanoes
- 2072, Quebraditas fault (zone)
- 2108a, Socorro Canyon fault zone, northern section
- 2108b, Socorro Canyon fault zone, southern section
- 2109, La Jencia fault
- 2109a, La Jencia fault, northern section
- 2109b, La Jencia fault, southern section
- 2110, West Joyita fault zone
- 2111, Cliff fault
- 2112, Loma Blanca fault
- 2113, Loma Pelada fault
- 2114, Coyote Springs fault
- 2115, Unnamed intrabasin faults west of Rio Puerco
- 2116, Sabinal fault
- 2117, Unnamed faults on the Llano de Manzano
- 2118, Los Pinos fault
- 2119, Manzano fault
- 2120, Hubble Spring fault
- 2121, Intrabasin faults on the Llano de Albuquerque
- 2122, Cat Mesa fault
- 2123, Santa Fe fault
- 2124, Unnamed faults near Mountair
- 2128, Coyote fault
- 2135, McCormick Ranch faults
- 2142, Faults west of Cochiti Pueblo
- 2143a, Unnamed faults of Jemez Mountains, Valles caldera section (Class B)[3]
- 2143b, Unnamed faults of Jemez Mountains, Toledo caldera section (Class B)[3]
- 2143c, Unnamed faults of Jemez Mountains, caldera margin section (Class B)[3]
- 2143d, Unnamed faults of Jemez Mountains, intracaldera section (Class B)[3]

Faults from Koning et al. (2004a)

- A2007a, Embudo fault system, northeastern section
- A2007b, Embudo fault system, southwestern section (replaces 2007b)
- A2007b, Embudo fault system, southwestern section, approximately located (replaces 2007b)
- A2007b, Embudo fault system, southwestern section, concealed (replaces 2007b)
- A2144, Ojo Caliente fault
- A2145, Chili fault

[2] URL: http://earthquake.usgs.gov/regional/qfaults

[3] Not included in the seismic hazard analysis

Earthquake Epicenters

- No Measure

Magnitude

- <= 3.0
- 3.1 - 4.0
- 4.1 - 5.0
- 5.1 - 6.0

URS	LANL PSHA Update Project No. 24342433	Historical Seismicity (1849 - 2005) and Quaternary Faults in the LANL Region	Plate 1

URS Corporation L:\Projects\Los_Alamos\MXD\Current Working Documents\Plate 3 Pajarito Regional with Seismicity update 030706.mxd Date: 3/6/2007 12:59:20 PM Name: dhwright0

Inset - Trench Location Detail

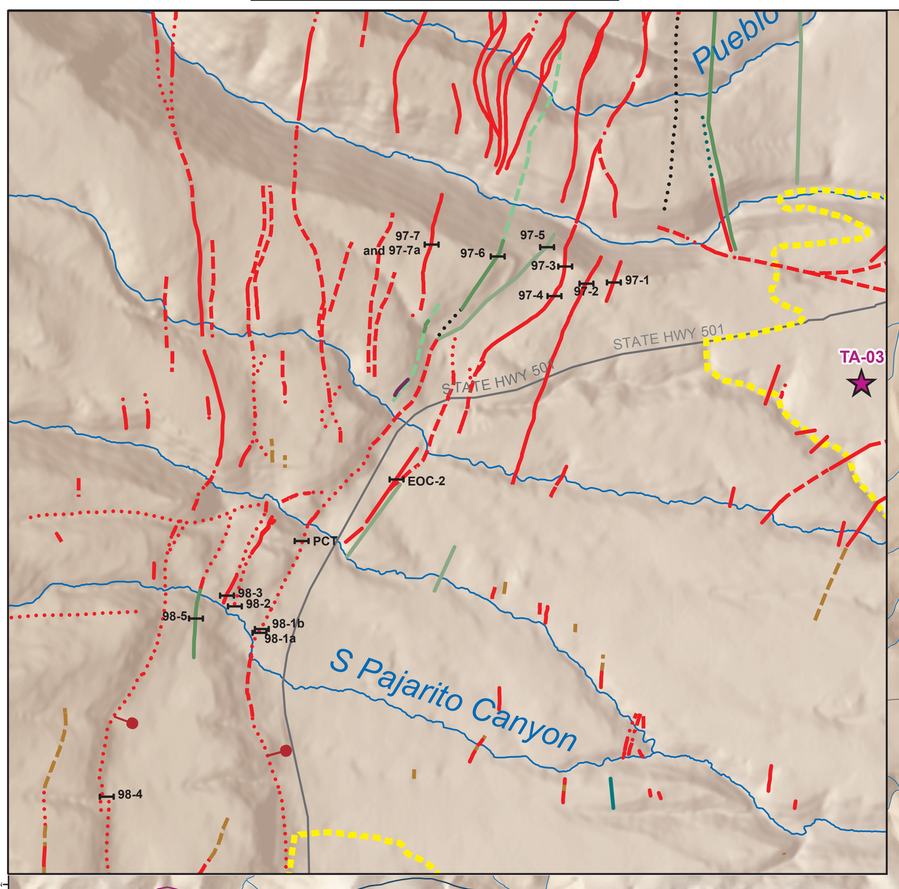

Pajarito Fault System (A2008)[1] (modified from Lewis et al., 2005)

- fault
- fault (assumed/uncertain)
- fault (concealed)
- fault (located approximately)
- fault zone
- fissure
- fissure (located approximately)
- monocline, bottom hinge
- monocline, bottom hinge (approximate)
- monocline, bottom hinge (concealed)
- monocline, top hinge
- monocline, top hinge (approximate)
- monocline, top hinge (concealed)
- syncline
- Fault from Machette et al. (1988), originally included as 2124, but included here as part of A2008

[1] Replaces faults: 2008 (Pajarito), 2026 (Rendija Canyon), 2027 (Guaje Mountain) and 2028 (Sawyer Canyon) of Machette et al. (1998)

Faults from the USGS Quaternary Fault Database [2]

- 2004, Lobato Mesa fault zone
- 2005, La Canada del Amagre fault zone
- 2006, Black Mesa fault
- 2007a, Embudo fault zone, northeastern section (Partially replaced with A2007a from Koning et al. 2004)
- 2009, Puye fault
- 2010, Pojoaque fault zone
- 2032, La Bajada fault
- 2142, Faults west of Cochiti Pueblo
- 2143a, Unnamed faults of Jemez Mountains, Valles caldera section (Class B)[3]
- 2143b, Unnamed faults of Jemez Mountains, Toledo caldera section (Class B)[3]
- 2143c, Unnamed faults of Jemez Mountains, caldera margin section (Class B)[3]
- 2143d, Unnamed faults of Jemez Mountains, intracaldera section (Class B)[3]

Faults from Koning et al. (2004a)

- A2007a, Embudo fault system, northeastern section
- A2007b, Embudo fault system, southwestern section (replaces 2007b)
- A2007b, Embudo fault system, southwestern section, approximately located (replaces 2007b)
- A2007b, Embudo fault system, southwestern section, concealed (replaces 2007b)
- A2144, Ojo Caliente fault
- A2145, Chili fault

[2] URL: http://earthquake.usgs.gov/regional/qfaults
[3] Not included in the seismic hazard analysis

TA-3 ★ Site Where Ground Motions Hazard is Calculated
WETF-2C ○ Borehole
SHT-1 ⊢ Trench

0 1 2 3 Kilometers

N

URS

LANL PSHA Update
Project No. 24342433

Map of the Pajarito Fault System and Nearby Faults

Plate 2